A new nuclear database for proton therapy applications

B. Braunn[1], A. Boudard[1], J. C. David[1], A. Koning[2], A. Leprince[1] and S. Leray[1]

[1] CEA, Centre de Saclay, IRFU/SPhN, F-91191 Gif-sur-Yvette, France

[2] Nuclear Research and Consultancy Group NRG, PO Box 25, 1755 ZG Petten, The Netherlands

E-mail: benjamin.braunn@gmail.com, jean-christophe.david@cea.fr

Abstract.

In this article, a new nuclear database for proton therapy applications is proposed. The building of this new database is part of the PROUESSE project which aims at developing a fast and reliable Monte Carlo code for proton dose calculation. In the first section, a review of the existing nuclear databases is done and their limitations identified. The new library is built using the TALYS 1.4 code with default parameters except for the three most important nuclei in proton therapy, ^{12}C, ^{16}O, ^{40}Ca, for which parameters have been adjusted to better fit with available experimental data. Comparisons to results obtained with the INCL intranuclear cascade model are also shown. The database contains the angular elastic distributions, non-elastic cross-sections, production cross-sections for all secondary particles produced and their outgoing energy spectra from 1 MeV to 249 MeV. Sixty nuclei of importance in proton therapy applications have been computed. An evaluated data file for hydrogen has also been produced using NN-Online data. Finally, comparisons between experimental depth-dose profiles in water and MCNPX simulations using our new database, another existing one and the INCL nuclear model are presented.

PACS numbers: 87.10.Rt, 87.55.Gh, 87.55.D-

1. Introduction

With 35 facilities in operation worldwide and 20 more in construction or planned‡, proton therapy is now an important tool to treat cancerous tumours. In France, "l'Institut Curie - Centre de Protonthérapie d'Orsay" (CPO) has recently shut-down its old 201 MeV synchrocyclotron and replaced it with a new 230 MeV cyclotron and a new treatment room with an isocentric arm has been built. "Le Centre Antoine Lacassagne", the second proton therapy centre in France (Nice), is also planning to acquire a 230 MeV cyclotron. It is scheduled to be operational in late 2013. And finally, the "Etoile" centre in Lyon should offer proton and carbon ion beams as solution to patients' treatments.

In parallel with the increasing capacity in charged particle therapy centres, a continuous effort to improve the effectiveness of this technique is undertaken, for example, in online beam imaging/control and in simulation tools to prepare treatments. These simulation tools named Treatment Planning Systems (TPS) are designed to provide the most appropriate dose delivery to the patient's pathology. Currently, TPS are using analytical codes like pencil beam algorithms ((Petti 1992), (Hong et al. 1996), (Szymanowski et al. 2001)) which are fast and accurate in homogeneous configurations. However, with more complicated heterogeneous geometries, their predictive power deteriorates and more accurate codes are needed. With the increasing CPU power, Monte Carlo (MC) based codes like MCNPX (Pelowitz 2011), GEANT4 (Agostinelli et al. 2003) or FLUKA (Batistoni et al. 2006) emerge as an alternative for clinical applications. A full Monte Carlo dose calculation code has already been implemented in a TPS (Paganetti et al. 2008). Yet, it still requires a long calculation time to compute 3D dose distributions compared to standard pencil beam codes. To circumvent this problem, fast pseudo-Monte Carlo algorithms ((Li et al. 2005), (Yepes et al. 2009)), simplified Monte Carlo methods ((Sakae et al. 2000), (Hotta et al. 2010)) as well as optimization (Grevillot et al. 2011)) have been proposed. The PROUESSE project (PROUESSE 2009) aims at developing a fast and reliable MC code for proton induced dose calculations to be implemented in TPS in replacement of analytical codes. The main challenge of this project is to decrease the computer time calculation while maintaining the reliability. This new code based on the Monte Carlo code PENELOPE (Salvat et al. 2006) is

‡ See the PTCOG website for the complete list.

upgraded to take into account the propagation of incident protons from 1 to 250 MeV into matter. This code handles both the electromagnetic interactions responsible for the slowing down of the proton beam by multiple scattering and thus for the position of the Bragg peak, and the nuclear interactions along the path of particles leading to a decrease of the dose in the Bragg peak and an increase along the path to the tumour. Concerning the multiple scattering, new mathematical algorithms (Tola & Garcia-Hernandez 2012) have been developed to enhance the speed of transport and energy deposition of the particles. This work will not be detailed here.

Regarding nuclear reactions, an optimization can be achieved by neglecting transport and interaction of secondary particles that do not play a significant role in the dose delivery. In several papers ((Stankovskiy et al. 2007), (Zacharatou-Jarlskog & Paganetti 2008), (Pia et al. 2010)) contributions of the different particles inducing a nuclear reaction have been quantified in the case of realistic depth-dose profiles. It appears that secondary light charged particles (p, d, t and α) generally contribute to less than 2% to the longitudinal dose, which is comparable to other experimental uncertainties. However, they can play a significant role in the lateral spreading of the dose (Pia et al. 2010). In the PROUESSE code, d, t and α are not transported; their energy is deposited at the production location in the same way as the heavy fragments. Neutron contribution to the dose is even smaller (of the order of 0.1%) and therefore transport and energy deposition of neutrons can safely be neglected.

In particle transport codes, nuclear reactions can be handled either by nuclear models or by data libraries. Models usually consist of the coupling of an entrance model covering the dynamical part of the collision (intranuclear cascade (INC) or quantum molecular dynamics (QMD) models) and a statistical model dealing with the de-excitation of the nucleus. Another way to handle the nuclear interactions is to use nuclear databases generated by more sophisticated reaction model codes, such as TALYS (Koning et al. 2008) or GNASH (Young et al. 1996), having a large number of parameters that can be adjusted against experimental data. Databases used in proton therapy already exist and reduce the calculation time but do not cover the energy range (0-250 MeV) of the most recent proton therapy facilities. In addition they do not include all nuclei existing in the human body. Finally, (Seravalli et al. 2012) shows that good evaluated nuclear databases are also useful in proton therapy PET-imaging where a good estimation of the production of β^+ emitters like ^{11}C and ^{15}O are mandatory to obtain correct β^+ production rates with Monte Carlo codes.

This article presents the work done to build a new nuclear database for proton therapy applications, originally dedicated to the PROUESSE code but which may be used by other codes as well. In the section 2, a review of the existing nuclear databases is done and their limitations pointed out. In the section 3, the principal characteristics of this new database are discussed. An evaluation of the non-elastic cross-sections, responsible for the attenuation of the primary beam, is done against experimental data for the ^{12}C, ^{16}O and ^{40}Ca nuclei. An extensive comparison of the total, differential elastic, and isotope production cross-sections with other existing evaluated nuclear databases is shown. For non-elastic and isotope production cross-sections, results obtained with the intranuclear cascade model INCL4.6 (Boudard et al. 2013) coupled with ABLA07 (Kelic et al. 2008) are also presented. The treatment of the proton-hydrogen reaction is detailed in a specific subsection. Finally, the last section is devoted to some comparisons between experimental measurements and calculations using the new database in MCNPX as a test of its validity.

2. State of the art

Originally, in Monte Carlo transport codes, reaction cross-sections and characteristics of the reaction products were provided by evaluated nuclear data libraries up to 20 MeV and above by nuclear models for neutron-induced reactions. For proton induced reactions, models were used at all energies. Recently, evaluated libraries have been extended to higher energies for neutron and proton induced reactions partly to speed up the codes, partly because libraries can be more easily adjusted to available experimental data. For instance, a major work has been done by the Los Alamos National Laboratory (LANL) in the late 1990's to provide to the nuclear application community an evaluated nuclear database for neutron and proton-induced reactions up to 150 MeV. This evaluated nuclear database, named LA150 (Chadwick et al. 1999), was mainly generated by the GNASH code (Young et al. 1996) and is now part of ENDF/B-VII(Chadwick et al. 2006). The part devoted to proton induced reaction (LA150h) contains data for 21 chemical elements (40 nuclei) and is commonly used by MCNPX.

In 2000, the Los Alamos group has also published another, more specific, database for the proton therapy applications in the ICRU report 63 (ICRU 2000). This database contains only evaluations for 11 nuclei from the LA150h database but with an extended energy range up to 250 MeV. Unfortunately it does not contains

evaluations for all possible nuclei in the human body and especially the evaluation of reactions on hydrogen. Since then, some works have been carried out to improve or extend these databases to other nuclei. For example, the TREF evaluation (Korovin et al. 2006) provides additional evaluated data for ^{23}Na, ^{nat}Mg and ^{nat}K up to 200 MeV. An extension of the LA150h hydrogen and oxygen evaluations up to 200 MeV has also been done by Stankovskiy in (Stankovskiy et al. 2008).

In 2008 a new evaluated library, TENDL, was released. This database gives evaluations for all isotopes from carbon to actinide nuclei with neutron and proton projectiles from 1 to 200 MeV. This evaluation is based on the TALYS code (Koning et al. 2008) and is updated each year. Like GNASH, TALYS is a collection of nuclear models put together to generate complete set of data for Monte Carlo codes. Unlike GNASH, the philosophy of TALYS is to reach completeness. This means that TALYS results are not necessarily fitted on experimental data before being moved to database. It is the price to pay to obtain a much more complete database: almost all the stable nuclei in TENDL while only 40 nuclei in LA150h.

However, none of these available databases are fully answering the needs corresponding to modern proton therapy facility, i.e. having a nuclear database for all the nuclei of interest for proton-induced reactions up to 250 MeV. Consequently, the decision has been made to generate a new evaluated database for this domain.

Since in transport codes nuclear models can be called instead of libraries, and in fact are called when libraries are not complete, it is worth investigating their prediction capability.

In INC models, the incident nucleon experiences a series of nucleon-nucleon collisions in the target nucleus, leading to the emission of fast particles and leaving an excited remnant nucleus, which is then handled by a de-excitation model. Typical combinations of INC-de-excitation models found in current transport codes are: Bertini-Dresner ((Bertini 1963), (Bertini 1969), (Dresner 1962)), INCL-ABLA ((Boudard et al. 2013), (Kelic et al. 2008)), or QMD-GEM ((Niita et al. 1995), (Furihata 2000)). Usually, it is considered that, because of the involved assumptions, INC models are valid only above 100-150 MeV. In fact, as shown in the recent benchmark of spallation models § and in (Boudard et al. 2013), they can give rather good results even below this limit. Unfortunately, all these models are CPU time consuming and have no flexibility in parameters to be adjusted to particular

§ http://www-nds.iaea.org/spallation

experimental data. In this paper, we used the last version of INCL-ABLA model, referred as INCL in the following, and compare its predictions to the experimental data and to adjusted models commonly used to produce evaluated databases.

3. A new evaluated nuclear database

We have used the TALYS 1.4 code to generate the new proton-nucleus reaction evaluation database required by PROUESSE because, according to the authors (Koning 2012), the models used in TALYS are in principle valid up to 250 MeV. In the case of proton-hydrogen reaction cross-sections, which cannot be obtained with TALYS, the on-line tool named NN-OnLine‖ has been used. A subsection is dedicated to this specific case.

This new database includes 23 different chemical elements (60 nuclei, listed in table 1, and extends from 1 MeV to 249 MeV¶, in table 2). It contains elastic angular distributions, non-elastic cross-sections, isotopic production cross-sections (excitation functions) for all secondary particles produced and their outgoing energy spectra.

The new evaluation is provided in ENDF-6 format file (ENDF 2007) thanks to the TEFAL code for TALYS calculations. Concerning the proton-hydrogen case, a home-made method is used to transform NN-OnLine values in ENDF-6 format. MF6/MT2 codification is used for the elastic angular distributions, MF3 for the non-elastic cross-sections, MF6/MT5 for the production cross-sections and outgoing energy spectra. The NJOY code (MacFarlane & Kahler 2010) allows to transform these files in ACE (A Compact ENDF) format files used by MCNPX (Pelowitz 2011) and also in ASCII files for PROUESSE. The table 3 summarizes the different steps to obtain the database files in each format.

3.1. Proton-Nucleus evaluation

For most of the nuclei, the standard parameters of TALYS remain untouched and the only modification compared to TENDL2011 is the extension up to 249 MeV. However, for the three main nuclei of importance in proton therapy, ^{12}C, ^{16}O and

‖ http://nn-OnLine.org

¶ For technical reasons, TALYS code cannot provide an evaluation at 250 MeV. The energy limit is 249 MeV.

Table 1: List of the nuclei included in the new database.

^{1}H	
^{12,13}C	^{36,38,40}Ar
^{14,15}N	^{39,40,41}K
^{16,17,18}O	^{40,42,43,44,46,48}Ca
^{19}F	^{46,47,48,49,50}Ti
^{23}Na	^{54,56,57,58}Fe
^{24,25,26}Mg	^{63,65}Cu
^{27}Al	^{127}I
^{28,29,30}Si	^{180,181}Ta
^{31}P	^{180,182,183,184,186}W
^{32,33,34,36}S	^{197}Au
^{35,37}Cl	^{204,206,207,208}Pb

Table 2: Energy grid used with TALYS to build the database. Five energy regions have been defined with low and high energy limits (E_{min} and E_{max} respectively) and energy bins δE. The values are in MeV.

E_{min}	E_{max}	δE
1	18	1
18	30	2
30	100	5
100	240	10
240	249	9

^{40}Ca, a careful verification against experimental data has been carried out. In the following, comparison of the non-elastic cross-sections, total cross-sections, elastic angular distributions and excitation functions for these three nuclei is presented. In each case, figures represent the experimental values (Exp. DATA) compared with the ICRU63 evaluation (ICRU) and with two TALYS evaluations: a first one with standard parameters (TALYS 1.4) and a second one (Modified TALYS)

Table 3: Steps to obtain the database files.

p + Nucleus	p + hydrogen
TALYS	NN-OnLine output
↓	↓
TEFAL	Fit by ROOT
↓	↓
ENDF-6 file	Legendre coefficients
↓	↓
NJOY	**ENDF-6 file**
↓	↓
↓	NJOY
↓	↓
ASCII & ACE	**ASCII & ACE**

with modified parameters obtained by iteratively tuning the surface and volume component of the imaginary part of the optical model potential developed by (Koning & Delaroche 2003). For non-elastic cross-sections evaluations, we show also INCL calculations.

3.1.1. Non-elastic cross-sections The non-elastic cross-section values are directly taken from the MF3/MT5 block of the ENDF-6 files for the three evaluations and from the EXFOR database (EXFOR/CSISRS 2012) for the experimental data. The figure 1 shows the non-elastic cross-sections as a function of the incident proton energy for the nuclei ^{12}C, ^{16}O and ^{40}Ca. In the three cases, the standard evaluation from TALYS overestimates experimental values from the threshold up to 100-150 MeV. Above, a slight underestimation is observed. A clear improvement of the shape of the distribution is obtained with the new evaluation which is compatible with the experimental data and comparable to the ICRU evaluation except that the peak appears at slightly too small energy. This could have some importance in dose calculation and explain some discrepancies in depth dose calculations (see section 4).

3.1.2. Total cross-sections Total cross-section values with respect to the incident energy are represented in figure 2. The values are taken from the ACE format file because the total cross-section is not directly provided in the ENDF-6 format. In the proton induced reaction case, the MF3/MT2 block of the ENDF-6 file does not store the elastic cross-section, but, according to the MF6/MT5 block, usually store the "nuclear plus interference cross-section" (ENDF 2007) (chapter 6). The experimental values, which are scarce, come from (Schwaller et al. 1979).

Qualitatively, the three evaluations are in agreement with the data. At low energies, the exponential increase of the cross-section is due to the Coulomb repulsive effect and is calculated with the Rutherford formula. In this region, the non-elastic part is negligible and no notable modifications are seen between the two TALYS evaluations. At higher energy, the Coulomb effects are less effective and the elastic and non-elastic cross-sections become comparable. The modification of the potential has little effects on the total cross-section evaluation. Except for ^{16}O, no significant improvement is noted between the two TALYS evaluations or with respect to ICRU evaluation. Since it is out of the scope of INC models to produce elastic scattering (no coherent NN interactions), no INCL calculations are presented.

3.1.3. Elastic angular distributions The figure 3 shows the differential elastic cross-section with respect to the scattering angle in the c.m. frame at 10, 45/50, 150 and 200/249 MeV. The values from the evaluation are stored in the MF6/MT2 block using the LAW5 LTP15 representation. See (ENDF 2007) for details. The experimental data come from the EXFOR database. Globally, the two TALYS evaluations are in good agreement with the experimental data at all angles and are consistent with the evolution of the distributions with the energy. The modifications of the potential in TALYS induces notable differences at low energy and rather important ones at large angle where the cross-section is small. In general, the new evaluation gives results slightly better than ICRU. In the case of ^{16}O the difference is larger and ICRU seems to have a problem at high energies and at backwards angles.

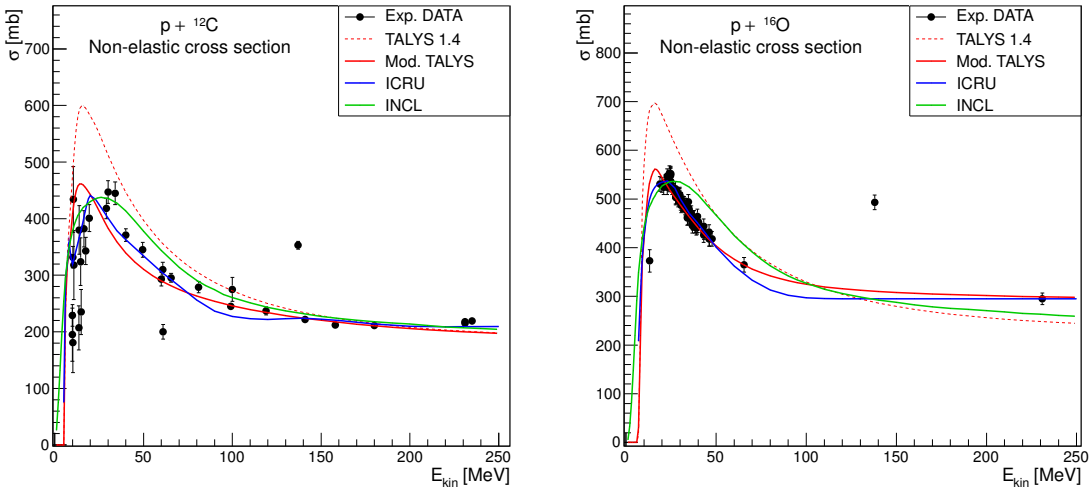

(a)

(b)

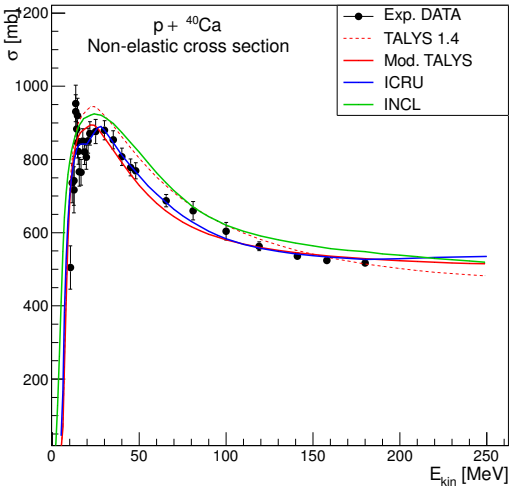

(c)

Figure 1: Non-elastic cross-section (in mb) as a function of the incident energy of the proton (in MeV) for the nuclei ^{12}C, ^{16}O and ^{40}Ca. Experimental DATA are represented in black dots, results of TALYS 1.4 with a dashed red line, Modified TALYS with a solid red line, ICRU with a solid blue line and INCL with a solid green line.

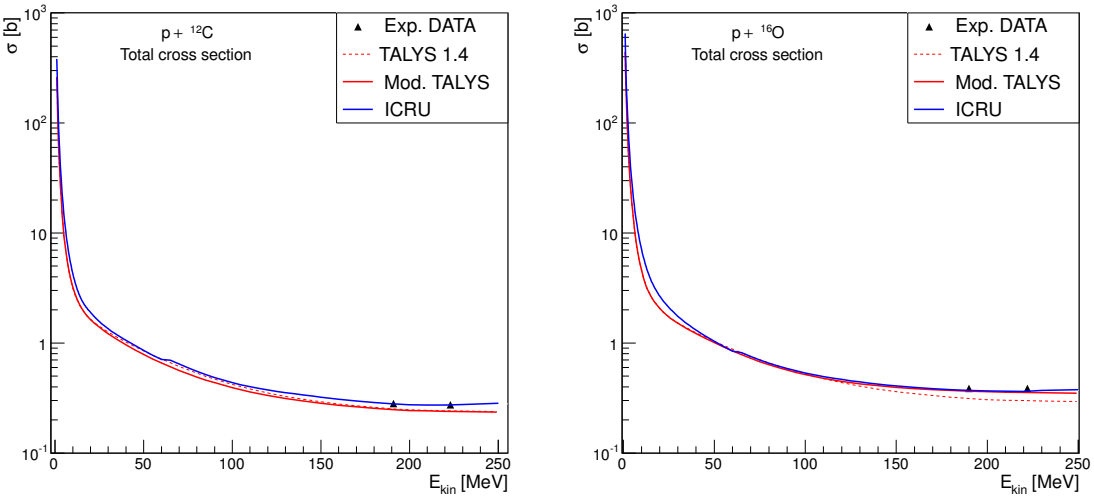

(a)

(b)

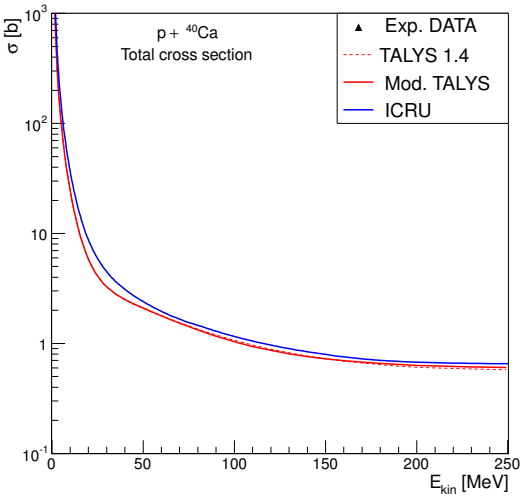

(c)

Figure 2: Total cross-section (in barn) as a function of the incident energy (in MeV). Experimental DATA are represented in black dots, results of TALYS 1.4 with a dashed red line, modified TALYS with a solid red line and ICRU with a solid blue line.

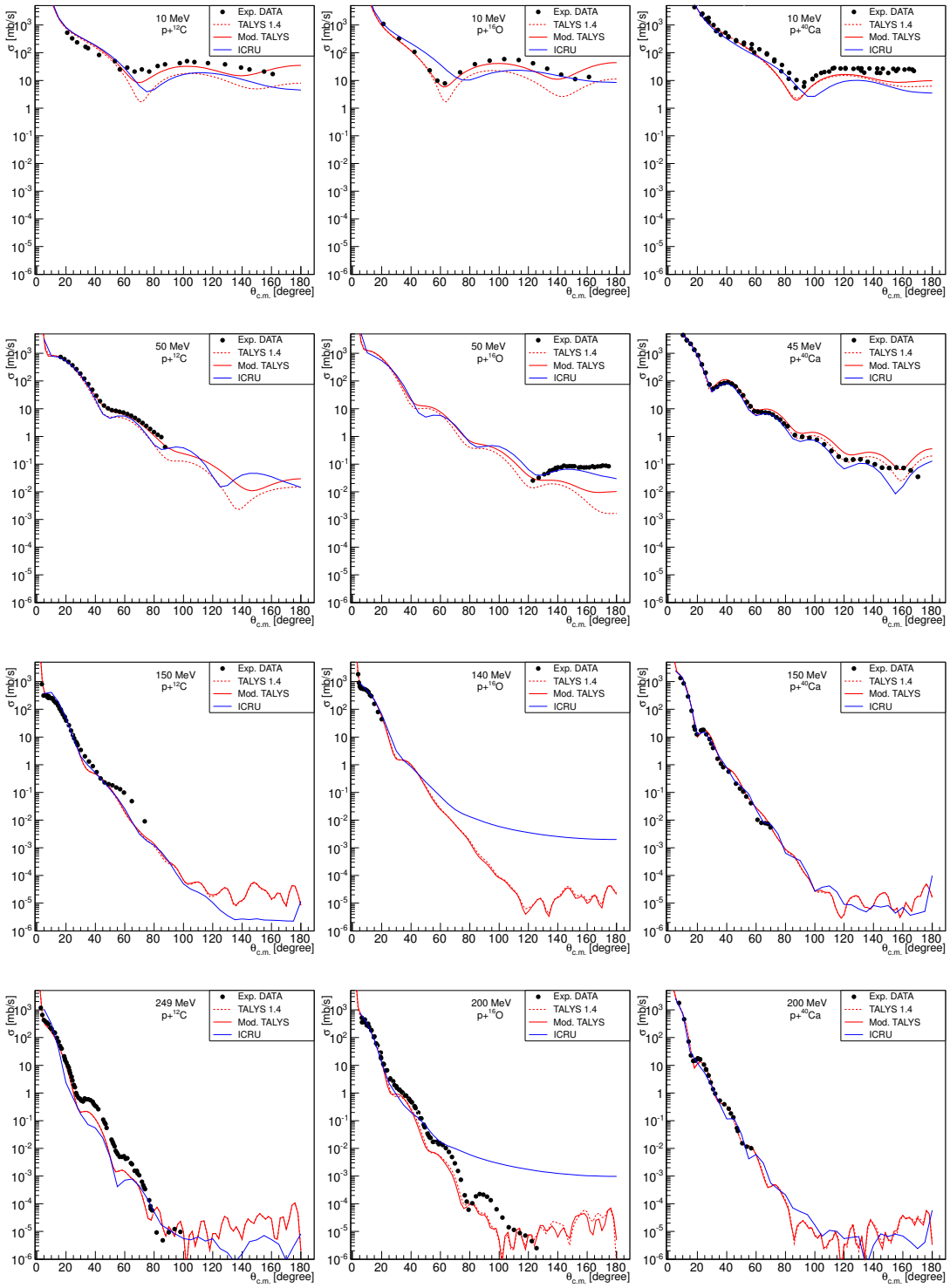

Figure 3: Differential elastic cross-sections (in mb/sr) as a function of the scattering angle in the centre of mass frame at 10, 45/50, 140/150 and 200/249 MeV. Experimental DATA are represented in black dots, results of TALYS 1.4 with a dashed red line, modified TALYS with a solid red line and ICRU with a solid blue line.

3.1.4. Isotopic production cross-sections The production rate of secondary particles produced by nuclear reactions may have some importance in the dose deposition both in the primary beam direction where the dose profile can be distorted and outside the beam where healthy tissues are to be spared from unwilling radiations. As discussed in the introduction, production cross-sections of some β^+ emitters are also of particular interest for PET imaging. More generally, comparing models to isotope production cross-sections allows testing its global consistency. This is why we present in figures 4, 5, 6, 7, 8 and 9 comparisons of the different models and evaluations to available experimental excitation functions, i. e. the production cross-sections as a function of incident energy for nucleons, composite particles (deuton, triton, helium 3 and helium 4) and various heavier fragments represented for ^{12}C, ^{16}O and ^{40}Ca targets. Results from INCL are also represented. Experimental data are taken from the compilation of (Iljinov et al. 1991).

Figures 4, 6 and 8 show the excitation functions for nucleons and composite particles up to ^{4}He. The different evaluations give a common general shape. Our modification of TALYS 1.4 has no significant effect on the excitation functions but clear differences are seen between TALYS, ICRU and INCL up to one order of magnitude in some cases. Anyway, due to scarce data, it is difficult to conclude on the best overall evaluation.

Figures 5, 7 and 9 show the excitation functions for nuclei heavier than ^{4}He. Comparisons are limited to existing experimental data. As observed previously, the different evaluations manage to reproduce the general shape of the experimental data. However, if we look in detail, none of the evaluations manage to reproduce with precision the experimental data for all the channels.

Most of the time too few sets of experimental data are available and sometimes they are in contradiction with each other. In few rare cases, enough experimental data are available on the 0-250 MeV range. Globally, INCL and ICRU seem to be more successful in reproducing the data than TALYS 1.4 or our modified TALYS.

We regroup on figure 10 three of these cases. It represents three reactions producing β^+ emitters from ^{12}C and ^{16}O target nuclei. Regarding ^{16}O(p,X)^{15}O and ^{12}C(p,X)^{11}C reactions, the old and new evaluations from TALYS fail to reproduce these excitation functions beyond the threshold. So far, although attempts to adjust the optical model, pre-equilibrium and level density parameters were done, it was not possible to improve the agreement. It seems that TALYS has clear difficulties to predict (p,pn) reactions far from threshold. This is not true only for light target but

seems to be the case also for ^{39}Ca as shown on figure 9 (bottom right).

On the other hand, INCL reproduces perfectly the ^{12}C(p,X)^{11}C reaction although it slightly overestimates the ^{16}O(p,X)^{15}O near the threshold. The ICRU evaluation is correct, but does not reproduce perfectly the two reactions either. ^{11}C can also be produced via ^{16}O(p,X)^{11}C, as shown in figure 10b. In this case, the modified TALYS evaluation appears to be the most reliable evaluation (except in the 50-100 MeV interval). These examples illustrate the difficulty to obtain overall good results due to complex and multiple mechanisms occurring in nuclear reactions. These codes should be carefully used in evaluations of secondary particle production rates because they are not yet very precise in the actual state of the art.

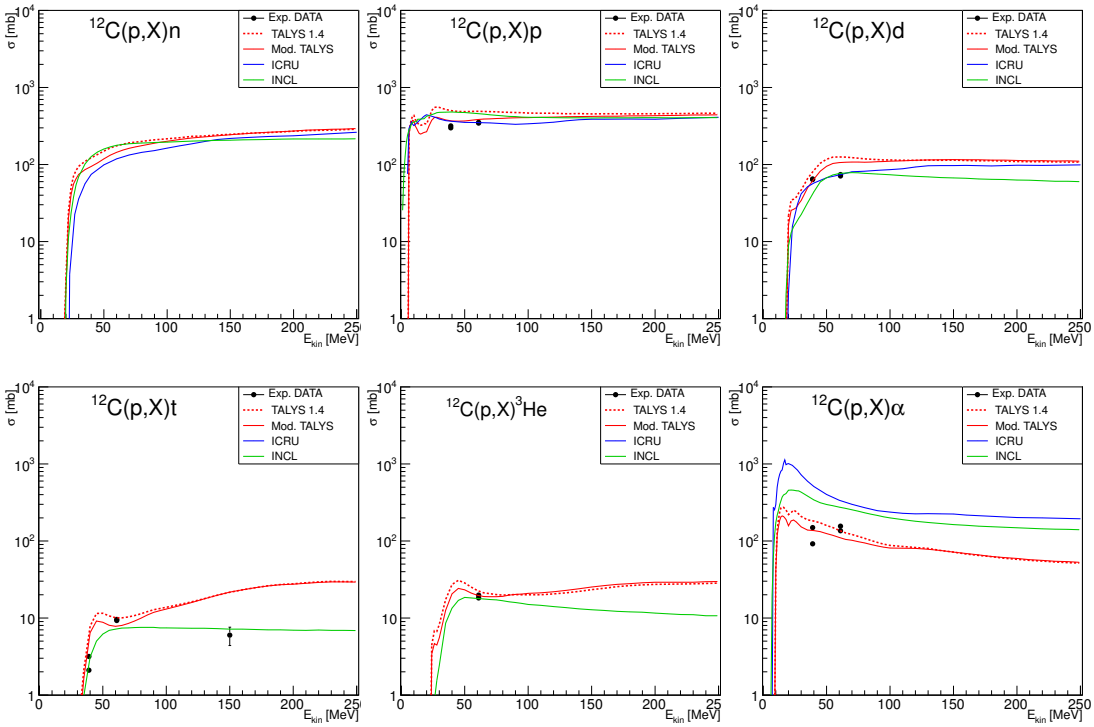

Figure 4: Production cross-sections for nucleons and composite particles (deuton, triton, helium 3 and helium 4) represented (in mb) as a function of the incident energy (in MeV) for ^{12}C targets. Experimental DATA are represented in black dots, TALYS 1.4 with a dashed red line, modified TALYS with a solid red line, ICRU with a solid blue line and INCL with a solid green line.

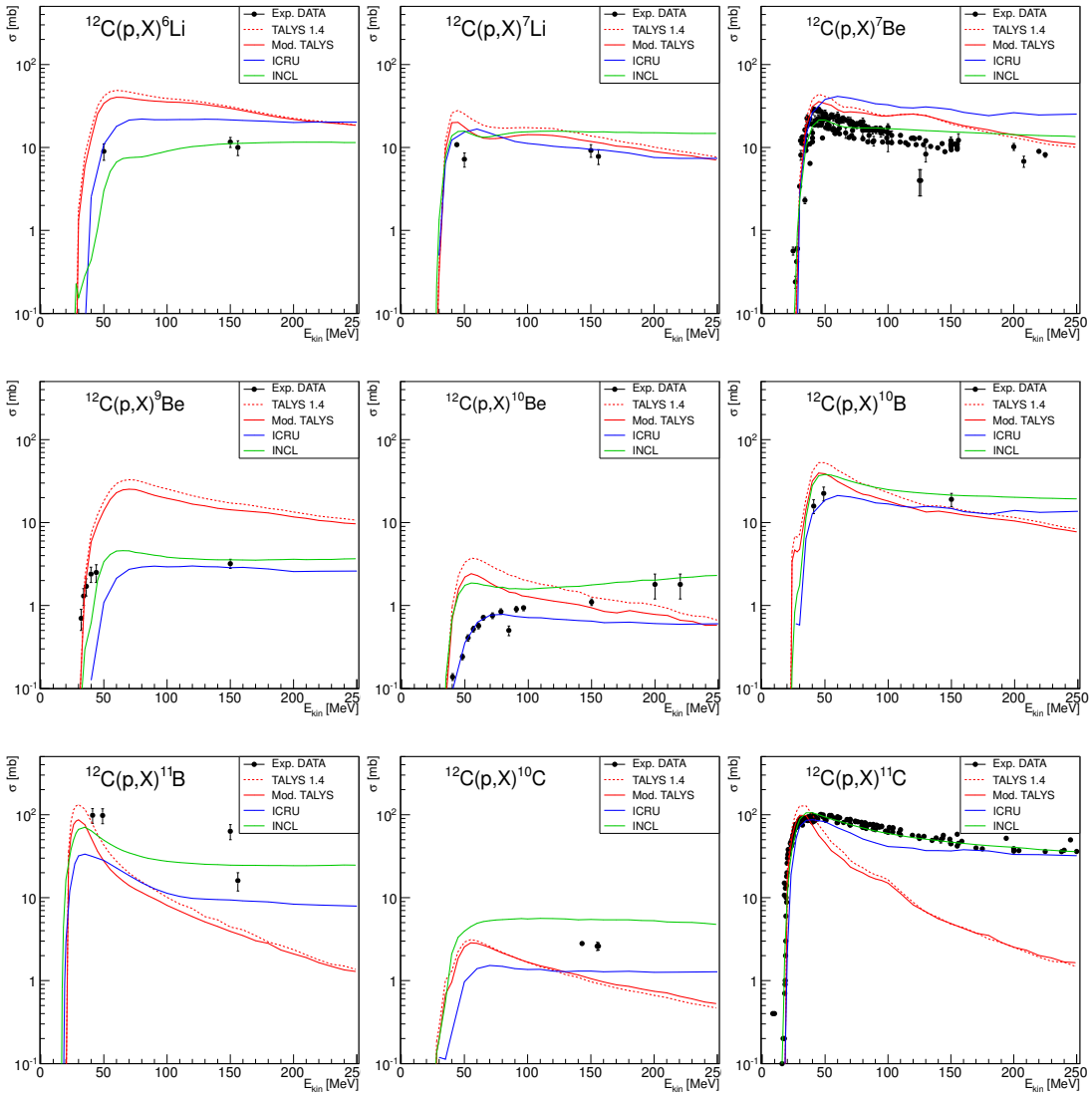

Figure 5: Production cross-sections for various heavier fragments represented (in mb) as a function of the incident energy (in MeV) for ^{12}C targets. Experimental DATA are represented in black dots, TALYS 1.4 with a dashed red line, modified TALYS with a solid red line, ICRU with a solid blue line and INCL with a solid green line.

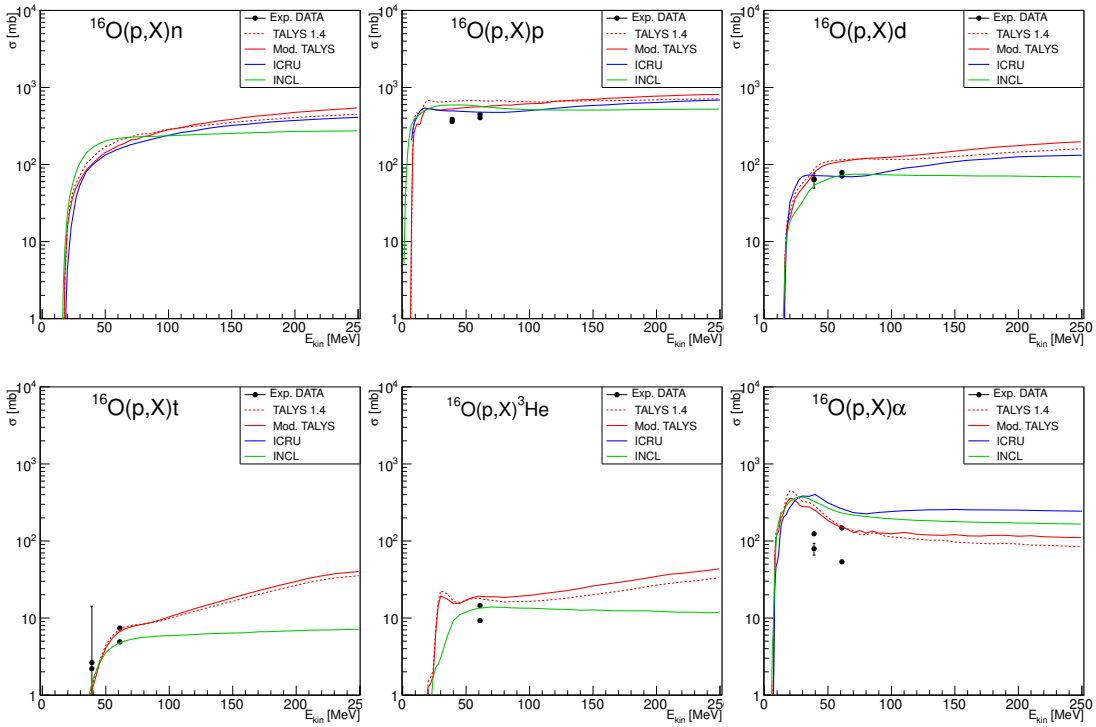

Figure 6: Production cross-sections for nucleons and composite particles (deuton, triton, helium 3 and helium 4) represented (in mb) as a function of the incident energy (in MeV) for ^{16}O targets. DATA are represented in black dots, TALYS$_{old}$ with a dashed red line, TALYS$_{new}$ with a sollid red line, ICRU with a solid blue line and INCL with a solid green line.

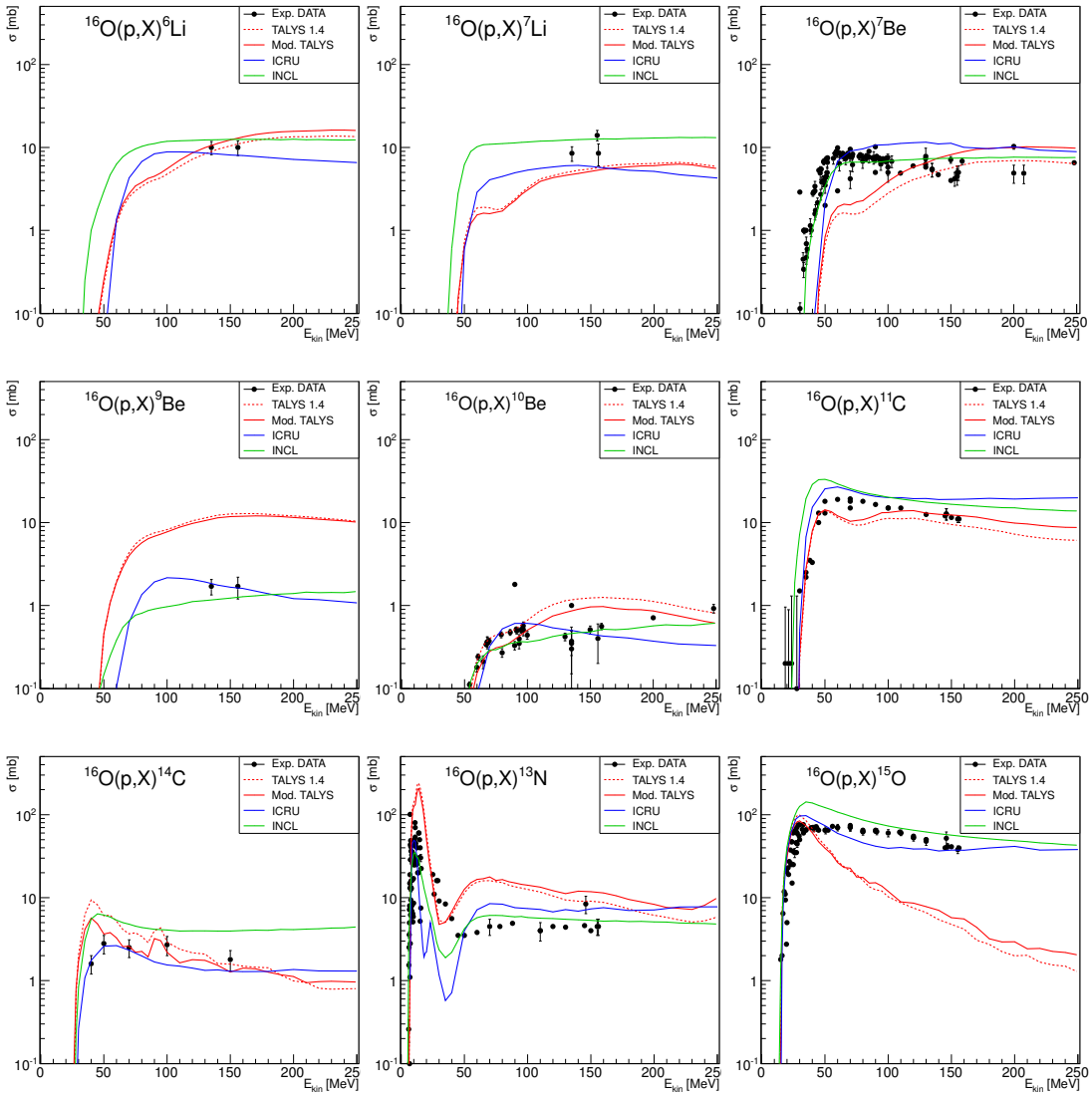

Figure 7: Production cross-sections for various heavier fragments represented (in mb) as a function of the incident energy (in MeV) for ^{16}O targets. Experimental DATA are represented in black dots, TALYS 1.4 with a dashed red line, modified TALYS with a solid red line, ICRU with a solid blue line and INCL with a solid green line.

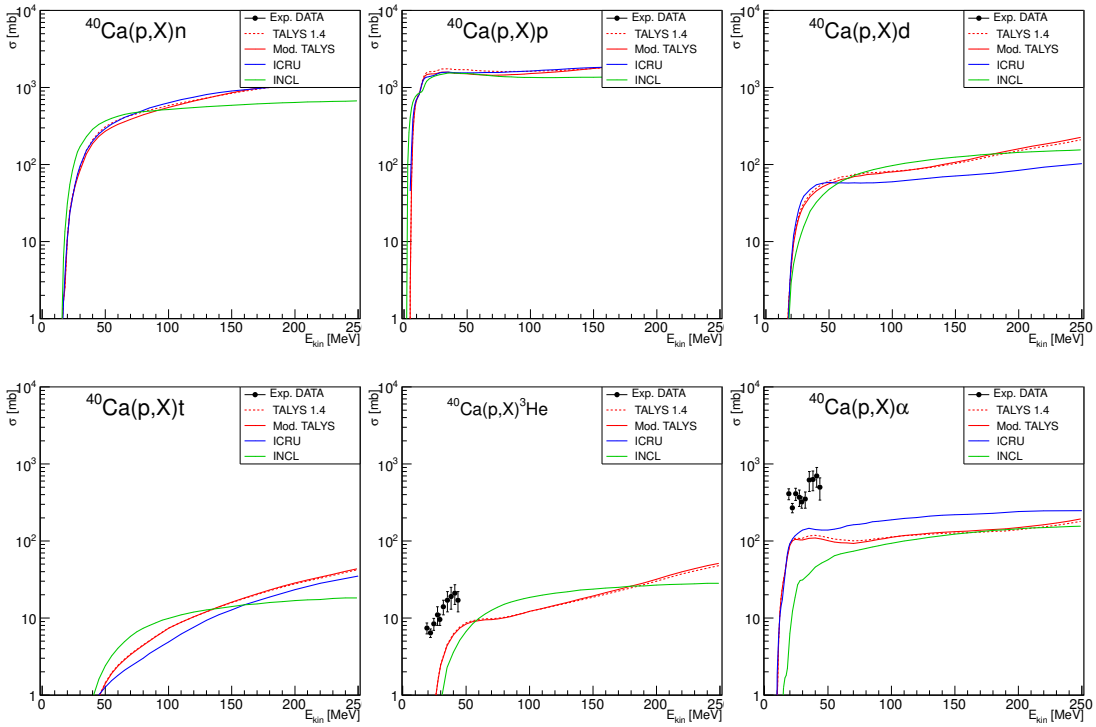

Figure 8: Production cross-sections for nucleon and composite particles (deuton, triton, helium 3 and helium 4) represented (in mb) as a function of the incident energy (in MeV) for ^{40}Ca targets. Experimental DATA are represented in black dots, TALYS 1.4 with a dashed red line, modified TALYS with a solid red line, ICRU with a solid blue line and INCL with a solid green line.

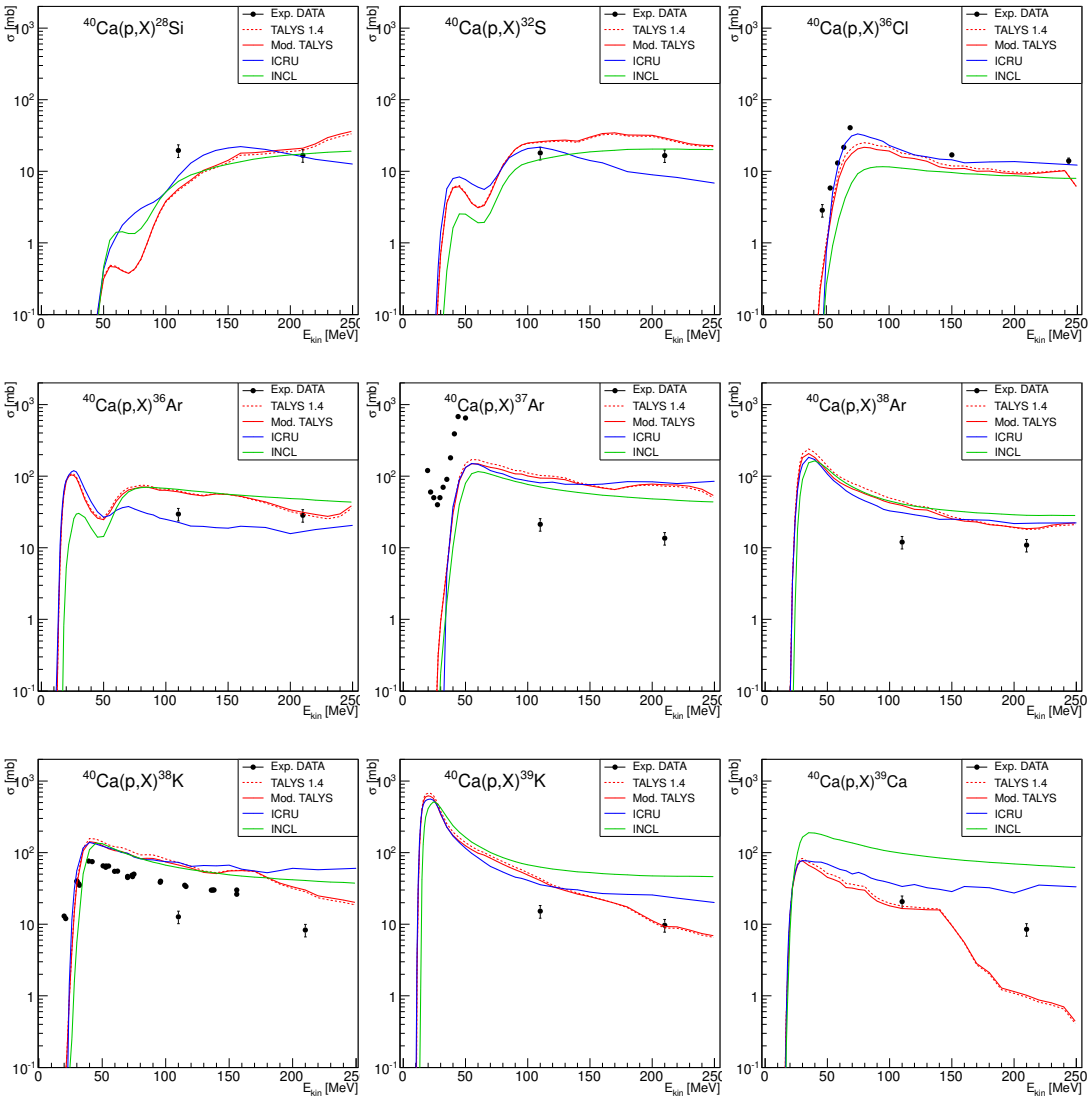

Figure 9: Production cross-sections for various heavier fragments represented (in mb) as a function of the incident energy (in MeV) for ^{40}Ca targets. Experimental DATA are represented in black dots, TALYS 1.4 with a dashed red line, modified TALYS with a solid red line, ICRU with a solid blue line and INCL with a solid green line.

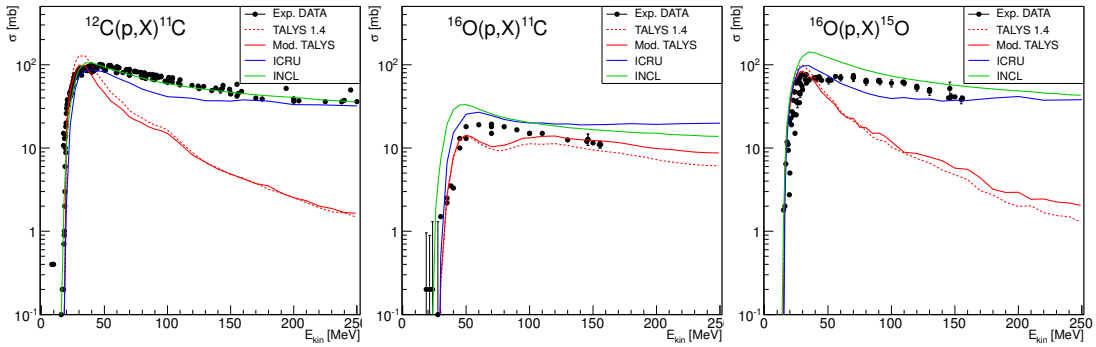

(a) (b) (c)

Figure 10: Production cross-sections (in mb) as a function of the incident energy (in MeV) for reactions producing β^+ emitters from ^{12}C and ^{16}O target nuclei. DATA are represented in black dots, TALYS$_{old}$ with a dashed red line, TALYS$_{new}$ with a solid red line, ICRU with a solid blue line and INCL with a solid green line.

3.2. Proton-hydrogen evaluation

The proton-hydrogen cross-section is a special case since it cannot be obtained with TALYS or with nucleon-nucleus codes. Specific nucleon-nucleon models are then used. In the energy range 1 - 250 MeV, pion production channel is not yet opened and therefore non-elastic processes can be neglected. This means that the total cross-section is the total elastic cross-section and is actually given by its angular differential cross-sections.

In LA150h, the evaluation has been made using the R-matrix analysis up to 150 MeV (Chadwick et al. 1999). Since this evaluation, an extension of this file has been attempted by fitting the elastic cross-section curve to 200 MeV using experimental data (see (Stankovskiy et al. 2008)). In the following figures, this extension will be named *Stankovskiy*. Recently, another phase shift analysis has been developed by (Moser et al. 2011) to represent differential elastic proton-proton scattering cross-sections with a better accuracy than ENDF. Unfortunately, the range of this analysis goes from 1.9 to 50 MeV only and their method is not extendable at higher energy. The ICRU report 63 does not give evaluation for this reaction.

3.2.1. Elastic angular distributions The new proton-hydrogen evaluation proposed here has been done using the tool developed by the Theoretical High Energy Physics Group of the Radboud University Nijmegen, NN-OnLine. It allows to compute the proton-proton differential cross-sections for energies from 10 keV to 350 MeV by means of different nucleon-nucleon interaction potentials. The elastic angular distribution values were obtained using the PWA93 (Stoks et al. 1993) potential available in the NN-OnLine tool. Different potentials are available and give similar results for this specific observable. These angular distributions were calculated for the energy grid given in table 2.

A fitting procedure using the Minuit package of the ROOT software (Brun & Rademakers 1997) and the formula described in the ENDF-6 manual (ENDF 2007) for the nuclear amplitude expansion representation (MF6/MT2 LAW5 LTP1) limiting the nuclear amplitude expansion to l=6 is used to obtain legendre coefficients. In a second step, these values are encoded in the "Legendre coefficients representation" used in the ENDF-6 format files.

The figure 11 shows the NN-OnLine, the Stankovskiy's and the LA150h evaluation at 50, 150 and 200 MeV compared with experimental data from (Berdoz et al. 1986), (Palmieri et al. 1958) and (Marshall et al. 1966) at 50.06, 147 and 213 MeV respectively. For 50 MeV, the three evaluations fit the experimental data. At 150 MeV, the NN-OnLine evaluation stands between LA150h and *Stankovskiy* and is slightly below the experimental data. This is compatible with the general trends of the distribution values decreasing with increasing kinetic energy in this region. The LA150h evaluation overestimates the experimental data while the *Stankovskiy* evaluation underestimates them. At 200 MeV, NN-OnLine gives an evaluation which reproduce accurately the experimental data while the *Stankovskiy* evaluation underestimates them by a factor of 2. An explanation will be given in the next section.

3.2.2. Total cross-section In principle, the total elastic cross-section is infinite due to the Coulomb repulsion. However, a "total elastic cross-section", excluding the Coulomb scattering, can be experimentally accessed by measuring $d\sigma/d\Omega$ at a scattering angle θ and integrated over the azimuthal angle ϕ as illustrated in (Chen et al. 1956). A compilation of experimental data are available in the particle data group (PDG).

The figure 12 shows the total elastic cross-section as a function of the kinetic

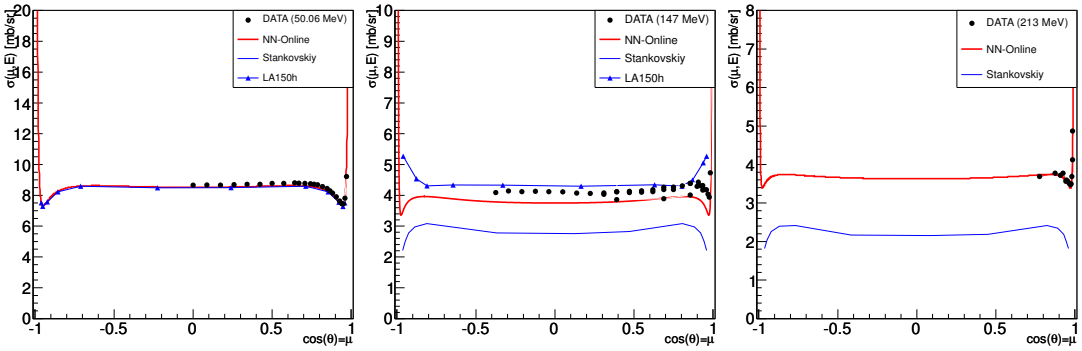

(a) 50 MeV (b) 150 MeV (c) 200 MeV

Figure 11: NN-OnLine, Stankovskiy and LA150h evaluations at 50, 150 and 200 MeV compared with experimental data from (A. Berdoz *et al*) at 50.06 MeV, (Palmieri *et al*) at 147 MeV and (J.F. Marshall *et al*) at 213 MeV.

energy for experimental data from the PDG and different evaluations.

In the ENDF-6 format codification, total cross-section for proton induced reactions are meaningless and values for σ_{tot} (MF3/MT=2) are arbitrarily set to 1 at all energies. So for the LA150h, the *Stankovskiy* evaluation and our NN-OnLine version, the cross-section values are taken from their equivalent ACE files. Unfortunately, ACE files do not take into account the indiscernibility of the particles (Goldberger & Watson 1975) and the values need to be divided by 2 to reproduce experimental data.

The figure 12 shows the comparison between experimental data and three different NN-OnLine evaluations. The first evaluation (NN-OnLine(90)) in thin solid blue line is obtained using the following formula:

$$\sigma_{tot} = 2\pi \cdot \frac{d\sigma}{d\Omega}\Big)^{NN}_{\theta_{c.m.}=90^\circ} \text{ given in (Chen et al. 1956).}$$

In thick solid (dashed-dotted) red line are represented the values from the ACE file (divided by 2). In the energy range from 5 to 250 MeV, the two evaluations give identical results and reproduce the experimental data (between 10 and 250 MeV). Moving from 5 to 1 MeV, the two evaluations diverge: the values from the formula are more or less a plateau around 1 barn while values from the ACE file follow the

general trend i.e. increasing with decreasing energy. This is due to the fact that the equation used begins to be inaccurate at low energy where Coulomb interactions cannot be neglected.

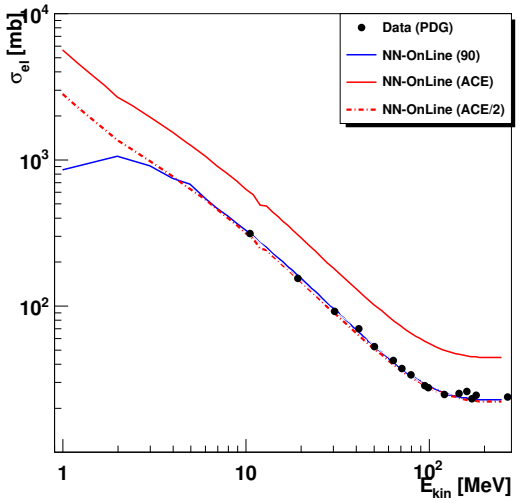

Figure 12: Proton-proton total elastic cross-section (in mb) as a function of the kinetic energy for experimental data from the PDG and NN-OnLine evaluation from different methods. NN-OnLine values from the equation are represented in solid blue line while the NN-OnLine values from the ACE file (divided by 2) are in solid (dashed-dotted) red line.

The figure 13a shows the comparison between the experimental data and the NN-OnLine, LA150h and Stankovskyi evaluations. From 1 MeV to 100 MeV the three evaluations are identical and reproduce the data. Beyond 100 MeV, discrepancies arise. LA150h and NN-OnLine succeed in reproducing the fact that the total cross-section values reach a valley around 20 mb, *Stankovskiy*'s evaluation fails, continuing to decrease with the energy. This is related to the discrepancies observed in the figure 11b where the angular distribution underestimate the experimental distribution.

The figure 13b shows also the comparison between the experimental data, the NN-OnLine evaluation, the INCL parametrization of the NN cross-section (Cugnon et al. 1996) and a NN cross-section parametrization available in the Geant4 transport

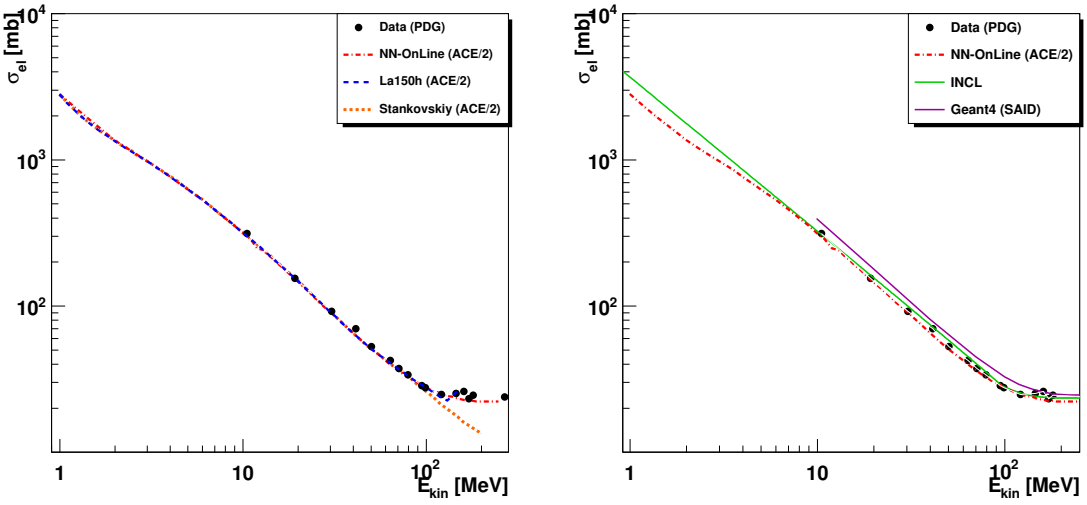

(a) (b)

Figure 13: Proton-proton total elastic cross-section (in mb) as a function of the kinetic energy for experimental data from the PDG and different evaluations 13a and nuclear codes 13b. NN-OnLine values from the ACE file divided by 2 are in dot-dashed red line. LA150h values are in dashed blue line, *Stankovskiy* values in dashed orange line, INCL values in green solid line and Geant4 values in purple solid line.

code (GEANT4 2010) which is derived from differential cross-sections obtained from the SAID [+] partial-wave analysis (Arndt et al. 2000).

The INCL parametrization is in good agreement with the experimental data when Geant4 values tend to overestimate them. INCL and NN-OnLine (ACE/2) give very good results and are equivalently close to the data. They diverge significantly at very low energy (below 6 MeV) where no experimental data are available. NN-OnLine (ACE/2) is the evaluation adopted for the new database.

[+] Scattering Analysis Interactive Dial-in

4. Validation of the new evaluated database

In this section the new database named Talys-based Evaluated Nuclear Data Library - Proton Therapy (TENDL-PT in the following) is compared with the ICRU database and the INCL nuclear model within MCNPX and validated against experimental depth-dose profiles. The simulations done with MCNPX used the proton and neutron "phys card" with "new vavilov" and "no recoil" options for hydrogen and default options for neutron. Comparisons have been performed with two sets of dose measurements. In the first part, experimental data obtained at the CPO Centre have been used, while the second part benefits from new data (Zhang et al. 2011) with proton energies below and above 150 MeV.

4.1. Proton beam on water - CPO measurement

Experimental values have been obtained at CPO with a standard beam set-up (Constant & De-Marzi 2012). The proton beam whose range in water is 15.5 cm, which corresponds approximately to an energy of 150 MeV, hits directly a water-phantom. An ionization chamber (CC13 Scanditronix Wellhoefer) has been used to collect the dose value inside the phantom.

Simulations of the depth-dose profiles have been carried out with MCNPX using the Phase-Space File (PSF) of the beam line provided by CPO. A cylinder corresponding to the CC13 (radius = 0.5 cm, thickness = 0.05 cm) has been used as integrating volume along the beam axis in the simulated water volume ($40 \times 40 \times 34.8$ cm^3). Phantom walls do not need to be simulated thanks to the experimental set-up which used a gantry directing the beam from above the water-phantom.

The figure 14 shows the comparison between depth-dose profile simulations of CPO experiment. Calculation results, blue and red lines, come from MCNPX simulations where the difference is the database (ICRU/TENDL-PT) or the nuclear model (INCL). Horizontal and vertical dashed line are drawn to help distinguish the maximum dose and the range at the Bragg peak. Concerning the figure 14a, ICRU and TENDL-PT are very similar on the whole depth. The point-to-point relative difference between the two simulations remains largely below 2% and the relative difference on the integrated energy is 0.9%. Concerning the figure 14b, it appears that INCL and TENDL-PT begin to provide different results only after mid-range in

depth. The difference between INCL and our database is probably due to differences in the reaction cross-section at low energy. Nonetheless, the choice of INCL or TENDL-PT induces less than 5% uncertainty all along the depth-dose profile and the relative difference on the integrated energy is 3.4%.

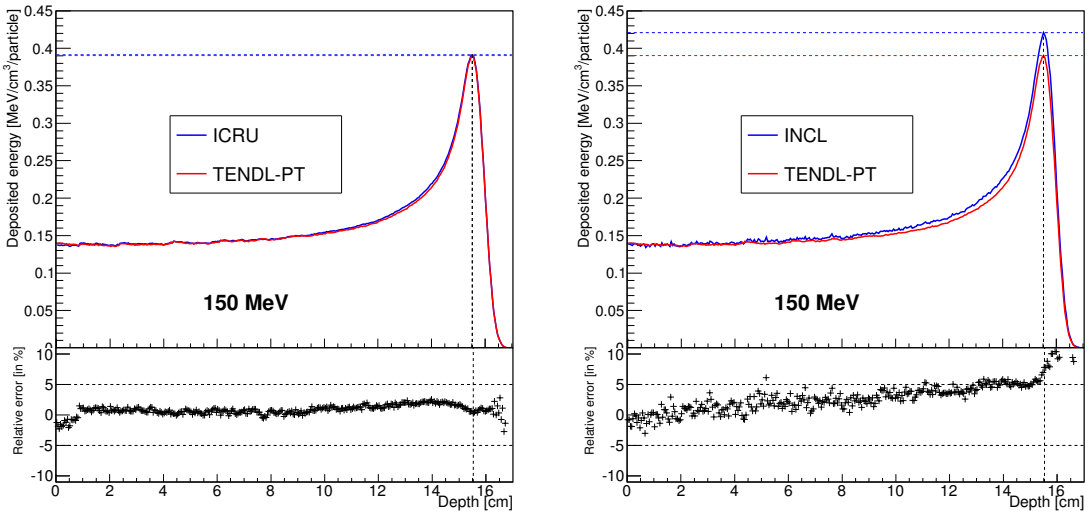

(a) (b)

Figure 14: Comparison between depth-dose profile simulations of CPO experiment (Constant E. & De Marzi L. 2012) using (a)ICRU/(b)INCL (in blue line) and TENDL-PT (in red line) at 150 MeV. The point-to-point relative difference between the simulation values is also shown.

The figure 15 represents the relative dose value as a function of the depth in water. Dose values are represented with black dots. Calculation results, blue and red lines, come from MCNPX simulations where the difference is the database or the nuclear model used. Since the experiment provide only relative values, a normalisation to the integral of the experimental depth-dose profile has been done. By doing so, only comparison of their shape is possible.

ICRU and TENDL-PT databases reproduce correctly the shape of the experimental Bragg curve except at the entrance of the phantom where the simulations values are above the experimental data. INCL, on the other hand, reproduce perfectly the experimental shape from the entrance up to the Bragg peak. At the Bragg

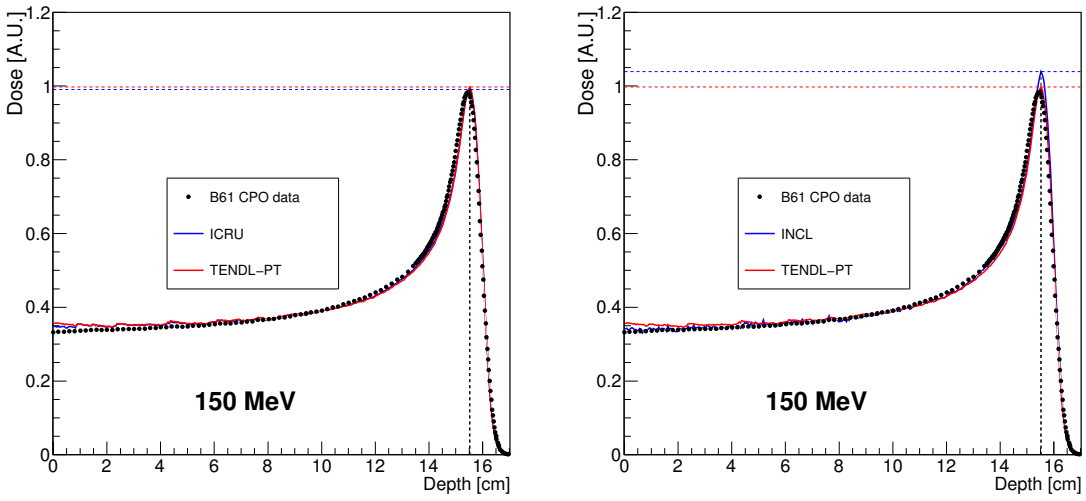

(a) (b)

Figure 15: B61 CPO experimental depth-dose profile data (Constant E. & De Marzi L. 2012) at 150 MeV compared with MCNPX simulation results using (a)ICRU/(b)INCL (in blue line) and TENDL-PT (in red line). Simulation calculations are normalised to the integral of the experimental data.

peak, however, INCL results are above the experimental data.

4.2. Proton beam on Water - data from (Zhang et al 2011)

Another series of comparisons have been done with depth-dose profile experimental data from (Zhang et al. 2011) at two different energies, below (121.2 MeV) and above (221.8 MeV) the energy used for the CPO measurement. The goal is to get an idea of the accuracy of our database at various energies and especially at higher energy.

For the MCNPX simulations, since little information on the beam has been given in (Zhang et al. 2011), we assume a mono-energetic beam with a Gaussian shape in space ($\sigma_{x,y} = 3$ mm). The simulated beam hits a water volume of $60 \times 60 \times 60$ cm^3 and a cylinder (matching the PTW-ionization chamber geometry: radius = 4.08 cm, thickness = 0.2 cm) has been used as integrating volume along the beam axis.

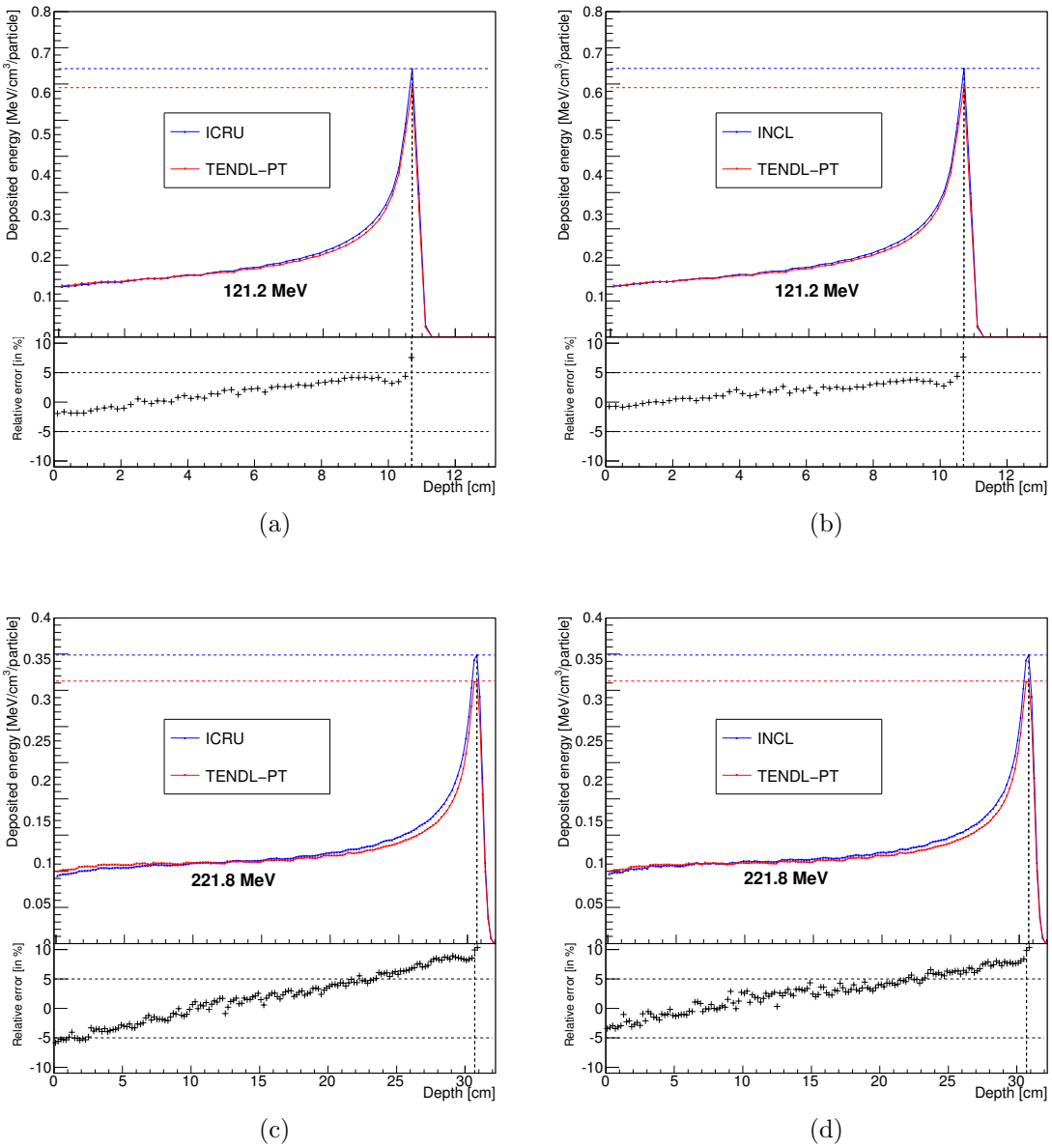

Figure 16: Comparison between depth-dose profiles simulations of (Zhang *et al* 2011) experiment using ICRU/INCL (in blue line) and TENDL-PT (in red line) at 121.2 (16a, 16b) and 221.8 MeV (16c, 16d). The point-to-point relative difference between the simulation values is also shown.

Figure 16 shows the comparison between depth-dose profile simulations of (Zhang et al. 2011). Calculation results, blue and red lines, come from MCNPX simulations where the difference is the database (ICRU/TENDL-PT) or the nuclear model (INCL). Horizontal and vertical dashed line are drawn to help distinguish the maximum dose and the range at the Bragg peak. For figures 16a and 16b, the main discrepancy between the simulations is located at the Bragg peak but the relative difference between the models remain below 5%. The relative difference on the integrated energy between ICRU (INCL) and TENDL-PT is 2.7 (2.9)%, respectively. At 221.8 MeV (see figs 16c and 16d), discrepancies are larger. TENDL-PT is over ICRU and INCL at low depth and below them around the Bragg peak and the relative difference between the models can reach locally 10%. The relative difference on the integrated energy between ICRU (INCL) and TENDL-PT is 3 (3.8)%, respectively. These relative differences reflect the influence of the nuclear databases or models used in the MCNPX transport code on the simulated depth-dose profiles.

Figure 17 represents the comparison between the depth-dose profile data from (Zhang et al. 2011) (in black dots) and results from MCNPX using the TENDL-PT database (in red line), the ICRU database or INCL model (in blue line) and normalised to the experimental integral dose. Concerning the figures 17a and 17b, ICRU and INCL reproduce with a slightly better accuracy than TENDL-PT the general shape of the depth-dose profile. TENDL-PT tends to be somewhat above the measurements at the entrance of the phantom and below them at the Bragg peak. We see also that the position of the Bragg peak is shifted towards higher depths by the simulations. This could be explained by the fact that we do not exactly know the details of the experimental conditions. At 221.8 MeV (see figs 17c and 17d), TENDL-PT results are largely above the experimental values at the entrance and below them at the Bragg peak. In contrast, INCL and ICRU results reproduce accurately the shape of the measured depth-dose profile from the entrance to the Bragg peak. From this comparison it appears that INCL and ICRU reproduce more accurately the experimental depth-dose profile shape than TENDL-PT. This is in contradiction with the results from the previous section. It could be due to the hypothesis we took to simulate the beam. A small modification in the beam energy or some additional layers of matter not mentioned before the water phantom could modified the simulated results. Finally, even if further investigations remain to be done, our new database reproduces experimental depth-dose profile shapes with a good accuracy on average for proton beam energies from 120 to 221 MeV.

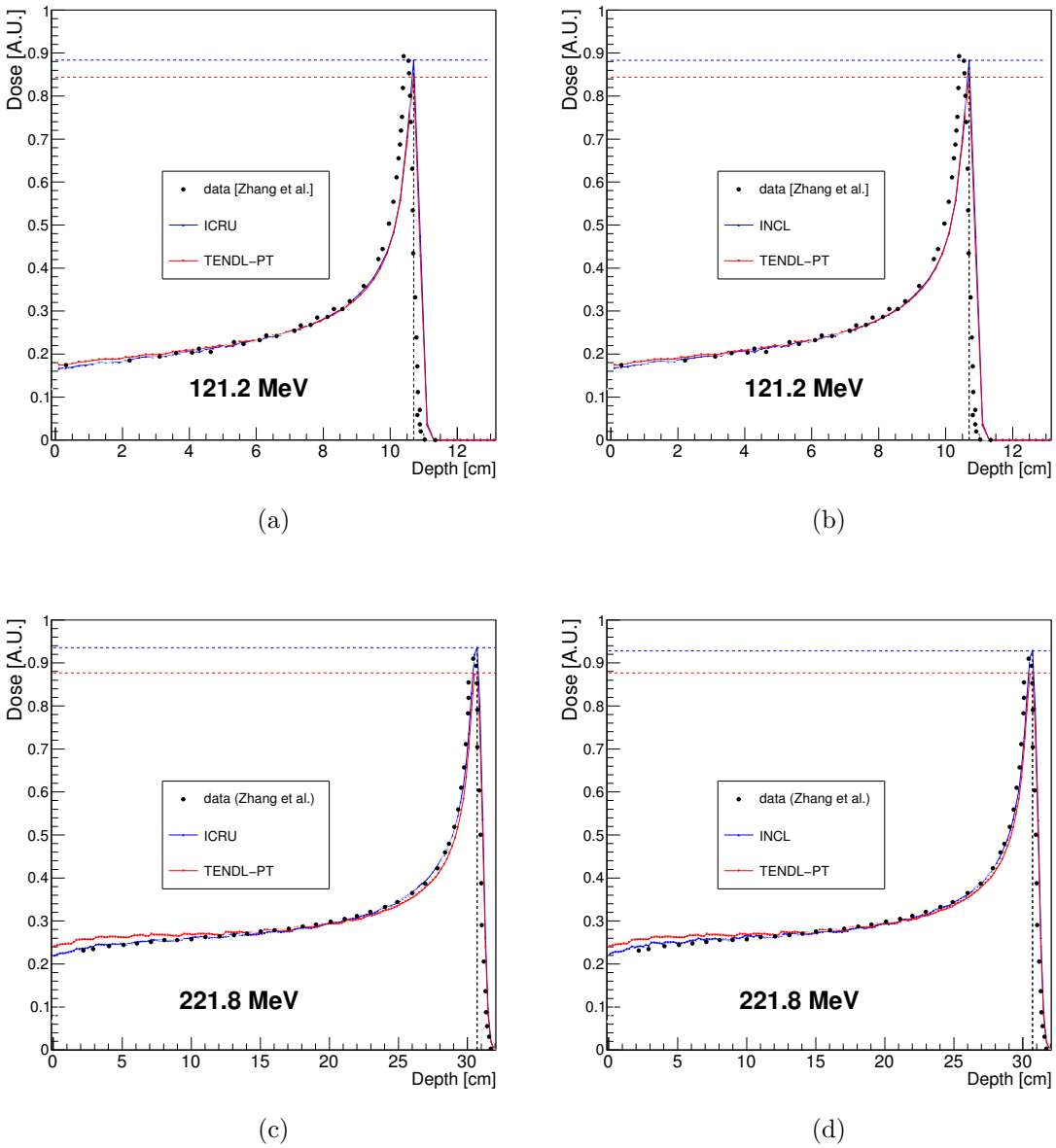

Figure 17: Experimental depth-dose profile data (Zhang *et al* 2011) at 121.2 MeV (17a, 17b) and 221.8 MeV (17c, 17d) compared with simulation results using (a,c) ICRU/(b,d) INCL (in blue line) and TENDL-PT (in red line). Simulation calculations are normalised to the integral of the experimental data.

5. Conclusion

A new proton-induced reaction database named TENDL-PT has been built using the TALYS code for proton-nucleus reactions and NN-OnLine for the proton-hydrogen reaction. This database is available in ENDF-6, ACE and ASCII format. It contains the angular elastic distributions, non-elastic cross-sections, production cross-sections for all secondary particles produced and their outgoing energy spectra for 60 target nuclei of importance in proton therapy applications in an energy range from 1 MeV to 249 MeV. Compared to existing libraries, TENDL-PT is either more complete or extending to higher energies, which is necessary in view of the arising of facilities with higher energy proton beams.

A careful verification against experimental data and a comparison with other nuclear databases and with results obtained with the INCL intranuclear cascade model has been performed for ^{12}C, ^{16}O and ^{40}Ca. This study showed the necessity of modifying slightly the default parameters of TALYS to improve the agreement in particular for the non-elastic cross-sections. Competitive results compared with other existing databases and with the INCL model have been obtained on various microscopic cross-sections. However, some discrepancies arise in particular cases but the lack of experimental data does not permit to conclude on the most accurate evaluation. In the specific case of β^+ emitters in the Carbon to Oxygen range, which is important for PET applications, the TALYS code, even after modifying the parameters, fails to reproduce the excitation functions while ICRU and INCL do. If TENDL-PT can be safely used for proton therapy applications, it has to be improved, especially on excitation functions, to become a multi-purpose library.

As examples of validation, two sets of simulations of experiments devoted to depth-dose profile measurements have been performed with MCNPX using the new database, ICRU and INCL. For CPO measurements at 150 MeV, results with the TENDL-PT database reproduce accurately the shape of the measured depth-dose profile. However, in the comparison with data from (Zhang et al. 2011), results with TENDL-PT do not fit perfectly the experimental shape both at 121 and 221 MeV. In the future, it should be interesting to perform comparisons with more detailed measurements (with absolute dose values and experimental uncertainties) to be able to conclude on the necessity (or not) to improve of the nuclear databases. This also allows an estimation of the error generated by changing only the nuclear reactions in these realistic depth-dose profile simulations. It appears that discrepancies in the

integrated deposited energy between TENDL-PT and ICRU or INCL remain below 4%. It reflects the uncertainties coming from the nuclear database and model used in MCNPX for depth-dose profile simulations.

Finally, TENDL-PT fulfils the PROUESSE project's criteria by providing nuclear data in the energy range of proton therapy applications (0-230 MeV) for sixty nuclei. This database is more complete than other existing nuclear databases and proves to be competitive with them and with the INCL nuclear model. Still, some improvements should be done in particular for the prediction of β^+ emitters.

This database is available in ENDF-6, ACE and ASCII format file on request.

Acknowledgments

This research is supported by the "Agence Nationale de la Recherche".

References

Agostinelli S et al. 2003 *Nucl. Instrum. Methods A* **506**(3), 250 – 303.

Arndt R A, Strakovsky I I & Workman R L 2000 *Phys. Rev. C* **62**, 034005.

Batistoni G, Muraro S, Sala P R, Cerutti F, Ferrari A, Roesler S, Fasso A & Ranft J 2006 *in* M Albrow & R Raja, eds, 'Proceedings of Hadronic Shower Simulation Workshop' Vol. 896 pp. 31 – 49.

Berdoz A, Foroughi F & Nussbaum C 1986 *Journal of Physics G: Nuclear Physics* **12**(6), L133.

Bertini H W 1963 *Phys. Rev.* **131**, 1801–1821.

Bertini H W 1969 *Phys. Rev.* **188**, 1711–1730.

Boudard A, Cugnon J, David J C, Leray S & Mancusi D 2013 *Phys. Rev. C* **87**, 014606.

Brun R & Rademakers F 1997 *Nucl. Instrum. Methods A* **389**(1-2), 81 – 86. New Computing Techniques in Physics Research V.

Chadwick M B et al. 1999 *Nuclear Science and Engineering* **131**(3), 293 – 328.

Chadwick M et al. 2006 *Nuclear Data Sheets* **107**(12), 2931 – 3060. Evaluated Nuclear Data File ENDF/B-VII.0.

Chen F F, Leavitt C P & Shapiro A M 1956 *Phys. Rev.* **103**, 211–225.

Constant E & De-Marzi L 2012. private communication.

Cugnon J, L'Hôte D & Vandermeulen J 1996 *Nucl. Instrum. Methods B* **111**(3-4), 215 – 220.

Dresner L 1962 *ORNL-TM-196* .

ENDF 2007 *ENDF-6 Formats Manual, Data formats and procedures for the Evaluated Nuclear Data File ENDF/B-VI and ENDF/B-VII.*

EXFOR/CSISRS 2012 *Experimental nuclear reaction data* IAEA - Nuclear data section.

Furihata S 2000 *Nucl. Instrum. Methods B* **171**(3), 251 – 258.

GEANT4 2010. Physics reference manual.

Goldberger M L & Watson K M 1975 *Collision theory* Robert E. Krieger publishing company, Huntington, New York.

Grevillot L, Bertrand D, Dessy F, Freud N & Sarrut D 2011 *Physics in Medicine and Biology* **56**(16), 5203.

Hong L, Goitein M, Bucciolini M, Comiskey R, Gottschalk B, Rosenthal S, Serago C & Urie M 1996 *Physics in Medicine and Biology* **41**(8), 1305.

Hotta K, Kohno R, Takada Y, Hara Y, Tansho R, Himukai T, Kameoka S, Matsuura T, Nishio T & Ogino T 2010 *Physics in Medicine and Biology* **55**(12), 3545.

ICRU 2000 *Nuclear Data for Neutron and Proton Radiotherapy and for Radiation Protection (Report 63)*.

Iljinov A S, Semenov V G, Semenova M P, Sobolevsky N M & Udovenko L V 1991 *Production of radionuclides at intermediate energies* Springer verlag, Berlin-Heidelberg.

Kelic A, Ricciardi M & Schmidt K H 2008 *Joint ICTP-IAEA Advanced Workshop on Model Codes for Spallation Reactions* pp. 181–222.

Koning A 2012. private communication.

Koning A & Delaroche J 2003 *Nuclear Physics A* **713**(3 - 4), 231 – 310.

Koning A, Hilaire S & Duijvestijn M 2008 *in* E Sciences, ed., 'Proceedings of the International Conference on Nuclear Data for Science and Technology - ND2007,' Vol. 1 pp. 211 – 214.

Korovin Y A, Konobeyev A Y, Pilnov G B & Stankovskiy A Y 2006 *Nucl. Instrum. Methods A* **562**(2), 721 – 724. Proceedings of the 7th International Conference on Accelerator Applications AccApp05.

Li J S, Shahine B, Fourkal E & Ma C M 2005 *Physics in Medicine and Biology* **50**(5), 1001.

MacFarlane R & Kahler A 2010 *Nuclear Data Sheets* **111**(12), 2739 – 2890. Nuclear Reaction Data.

Marshall J F, Brown C N & Lobkowicz F 1966 *Phys. Rev.* **150**, 1119–1122.

Moser M, Reichart P, Greubel C & Dollinger G 2011 *Nucl. Instrum. Methods B* **269**(20), 2217 – 2228. 12th International Conference on Nuclear Microprobe Technology and Applications.

Niita K, Chiba S, Maruyama T, Maruyama T, Takada H, Fukahori T, Nakahara Y & Iwamoto A 1995 *Phys. Rev. C* **52**, 2620–2635.

Paganetti H, Jiang H, Parodi K, Slopsema R & Engelsman M 2008 *Physics in Medicine and Biology* **53**(17), 4825.

Palmieri J, Cormack A, Ramsey N & Wilson R 1958 *Annals of Physics* **5**(4), 299 – 341.

Pelowitz D B 2011 *MCNPX 2.7.0 Extensions LA-UR-11-02295*.

Petti P L 1992 *Medical Physics* **19**(1), 137–149.

Pia M G, Begalli M, Lechner A, Quintirei L & Saracco P 2010 *IEEE Transactions on Nuclear Science* **57**(5), 2805.

PROUESSE 2009. PRotonthérapie : développement et validation dun OUtil de modélisation Et Simulation monte carlo précises et rapides du dépôt de doSE, ANR project ANR-09-COSI-010-05.

Sakae T, Nohtomi A, Maruhashi A, Sato M, Terunuma T, Kohno R, Akine Y, Hayakawa Y & Koike Y 2000 *Medical Physics* **27**(2), 368–373.

Salvat F, Fernández-Varea J M & Sempau J 2006 *PENELOPE-2006, A Code System for Monte*

Carlo Simulation of Electron and Photon Transport OECD ISBN 92-64-02301-1, Spain.

Schwaller P, Pepin M, Favier B, Richard-Serre C, Measday D & Renberg P 1979 *Nuclear Physics A* **316**(3), 317 – 344.

Seravalli E, Robert C, Bauer J, Stichelbaut F, Kurz C, Smeets J, Ty C V N, Schaart D R, Buvat I, Parodi K & Verhaegen F 2012 *Physics in Medicine and Biology* **57**(6), 1659.

Stankovskiy A, Kerhoas-Cavata S, Ferrand R & Nauraye C 2007 *in* 'Eighth International Topical Meeting on Nuclear Applications and Utilization of Accelerators' Vol. 1 pp. 349 – 356.

Stankovskiy A, Kerhoas-Cavata S, Ferrand R & Nauraye C 2008 *in* 'International Conference on Nuclear Data for Science and Technology 2007' Vol. 1 pp. 1387 – 1389.

Stoks V G J, Klomp R A M, Rentmeester M C M & de Swart J J 1993 *Phys. Rev. C* **48**, 792–815.

Szymanowski H, Mazal A, Nauraye C, Biensan S, Ferrand R, Murillo M C, Caneva S, Gaboriaud G & Rosenwald J C 2001 *Medical Physics* **28**(6), 975–987.

Tola F & Garcia-Hernandez J C 2012. private communication.

Yepes P, Randeniya S, Taddei P J & Newhauser W D 2009 *Physics in Medicine and Biology* **54**(1), N21.

Young P, Arthur E & Chadwick M 1996 *in* A Gandini & G Reffo, eds, 'proceeding of the IAEA workshop nuclear reaction data and nuclear reactors - physics, design and safety' World scientific puplishing, Ltd., Singapore (1998) p. 227.

Zacharatou-Jarlskog C & Paganetti H 2008 *IEEE Transactions on Nuclear Science* **55**(3), 1018.

Zhang X, Liu W, Li Y, Li X, Quan M, Mohan R, Anand A, Sahoo N, Gillin M & Zhu X R 2011 *Physics in Medicine and Biology* **56**(24), 7725.